TWO-DIMENSIONAL MODEL FOR THE SUBSONIC PROPAGATION OF LASER SPARKS

By

JAD HANNA BATTEH

A DISSERTATION PRESENTED TO THE GRADUATE COUNCIL OF
THE UNIVERSITY OF FLORIDA
IN PARTIAL FULFILLMENT OF THE REQUIREMENTS FOR THE
DEGREE OF DOCTOR OF PHILOSOPHY

UNIVERSITY OF FLORIDA

1974

To my wife, Jane,
and
to my parents

ACKNOWLEDGEMENTS

I would like to express my sincere gratitude to the members of my supervisory committee. In particular, my deepest appreciation is extended to the committee chairman Dr. Dennis R. Keefer, whose advice and guidance were essential to the completion of this endeavor.

I am indebted to Dr. Bruce Henriksen for suggesting the problem and for his continued interest in this research.

My gratitude for the criticism, encouragement and technical assistance of Mr. John Allen is exceeded only by my regard for his personal friendship. Finally, I am especially grateful to my wife for her diligent preparation of this manuscript.

TABLE OF CONTENTS

		Page
ACKNOWLEDGEMENTS		iii
LIST OF TABLES		v
LIST OF FIGURES		vi
NOMENCLATURE		viii
ABSTRACT		xii
CHAPTER		
I	INTRODUCTION	1
II	THEORETICAL DEVELOPMENT	7
III	SOLUTION OF THE EQUATIONS	16
IV	SIMPLIFIED ONE-DIMENSIONAL ANALYSIS	24
V	EXAMPLE CALCULATIONS	29
VI	DISCUSSION OF RESULTS	37
VII	CONCLUSIONS	44
APPENDIX		
I	CONVERGENCE OF THE SERIES SOLUTION	61
II	EFFECT OF RADIATION ON SUBSONIC SPARKS	64
REFERENCES		74
BIOGRAPHICAL SKETCH		77

LIST OF TABLES

Table		Page
I	Physical Properties of Laser Sparks of .15 cm and .50 cm Radius	60

LIST OF FIGURES

Figure		Page
1.	Co-ordinate System for the Steady State Propagation of a Laser Spark in a Channel . .	47
2.	Variation of c_p/λ with Temperature for Atmospheric-pressure Air	48
3.	Variation of Thermal Conductivity and Thermal Potential with Temperature for Atmospheric-pressure Air	49
4.	Incident Laser Intensity Required to Maintain a Spark as a Function of Channel Radius	50
5.	Isotherms for a Spark with R_L = .15 cm, R_c = 1.25 R_L and u = 0	51
6.	Isotherms for a Spark with R_L = .15 cm, R_c = 1.25 R_L and u =20 cm/sec	52
7.	Isotherms for a Spark with R_L = .50 cm, R_c = 1.25 R_L and u = 0	53
8.	Isotherms for a Spark with R_L = .50 cm, R_c = 1.25 R_L and u = 20 cm/sec	54
9.	Variation of the Thermal Conduction Parameter with R_c/R_L	55
10.	Axial Variation of the Volumetric Energy Loss Terms for R_L = .15 cm, R_c = 1.25 R_L and u = 0	56

Figure Page

11. Axial Variation of the Volumetric Energy Loss Terms for R_L = .15 cm, R_c = 1.25 R_L and u = 20 cm/sec 57

12. Axial Variation of the Volumetric Energy Loss Terms for R_L = .50 cm, R_c = 1.25 R_L and u = 0 58

13. Axial Variation of the Volumetric Energy Loss Terms for R_L = .50 cm, R_c = 1.25 R_L and u = 20 cm/sec 59

A.1 Isotherms for a Spark with R_L = .50 cm, R_c = 2 R_L, u = 1 m/sec and T_i = 6,000 ^oK . . 73

NOMENCLATURE

a_n	coefficient of the series solution
A	radial heat conduction parameter
A_n	coefficient of the series solution for θ_1 defined by Equation (3.8)
b_n	coefficient of the series solution
B_n	coefficient of the series solution for θ_2 defined by Equation (3.9)
c_n	coefficient of the series solution
c_p	specific heat capacity, joule/gm ^oK
C_n	coefficient of the series solution for θ_2 defined by Equation (3.10)
d	spark length, cm
e	electron
E_i	ionization potential, ev
f_n	axial function for the solution of θ_1
F_n	axial function for the solution of θ_h
g	Gaunt factor
g_n	radial function for the solution of θ_1
G_n	radial function for the solution of θ_h
h	Planck's constant, ev-sec
H(r)	Heaviside step function
J_o	zero order Bessel function of the first kind
J_1	first order Bessel function of the first kind

l_ν	mean free path of radiation of frequency ν , cm
L	characteristic spark dimension, cm
m	thermal radiation parameter, cm^{-2}
M_n	terms of the series used for comparison in the Weierstrass M-Test.
n	summation index
N_e	electron number density, cm^{-3}
N_+	positive ion number density, cm^{-3}
P_A	power absorbed by the spark, kW
P_o	incident laser power, kW
r	radial co-ordinate, cm
R_c	channel radius, cm
R_L	laser beam radius, cm
S	laser intensity, kW/cm^2
S_o	incident laser intensity, kW/cm^2
S_o'	incident laser intensity for a reduced ignition temperature, kW/cm^2
t_n	coefficient of the series solution
T	temperature, ^oK
T_e	electron temperature, ^oK
T_h	heavy-particle temperature, ^oK
T_i	ignition temperature, ^oK
$\bar{T}_m$	maximum value of the radially averaged temperatures, ^oK
T_n	$(A_n/x_{on})J_1(x_{on}R_L/R_c)$
u	spark propagation velocity, cm/sec
v_r	radial velocity component, cm/sec

v_x	axial velocity component, cm/sec
x	axial co-ordinate, cm
x_m	axial location of the maximum temperature, cm
x_{on}	n^{th} zero of J_o
Y_o	zero order Bessel function of the second kind
Z	ionic charge

α	$\rho_o c_p u / \lambda$, cm^{-1}
β_n^2	separation constant, equal to x_{on}^2/R_c^2, cm^{-2}
γ	$\left[1 + 4A/\alpha^2 R_L^2\right]^{1/2}$
γ'	$\left[1 + (4/\alpha^2 R_L^2)(m R_L^2 + A)\right]^{1/2}$
γ_n	$\left[1 + (2x_{on}/\alpha R_c)^2\right]^{1/2}$
γ_n'	$\left\{1 + (4/\alpha^2)\left[(x_{on}/R_c)^2 + m\right]\right\}^{1/2}$
$\delta_{1n,2n}$	exponential factors in the series solution, cm^{-1}
θ	thermal potential, kW/cm
θ_i	ignition thermal potential, kW/cm
θ_i'	reduced ignition thermal potential, kW/cm
θ_1	thermal potential in the region $x < 0$, kW/cm
θ_2	thermal potential in the region $x > 0$, kW/cm
θ_h	solution of the homogeneous equation for θ_2, kW/cm
θ_p	particular solution of the equation for θ_2, kW/cm
$\bar{\theta}$	thermal potential averaged over the laser radius, kW/cm

$\bar{\theta}_1$	radially averaged thermal potential in the region $x < 0$, kW/cm
$\bar{\theta}_2$	radially averaged thermal potential in the region $x > 0$, kW/cm
$\bar{\theta}_m$	maximum of the radially averaged thermal potentials, kW/cm
κ_ν	absorption coefficient for radiation of frequency ν, cm^{-1}
λ	thermal conductivity, kW/cm ^oK
λ_r	radiative conduction coefficient, kW/cm ^oK
ν	radiation frequency, sec^{-1}
ρ	density, gm/cm^3
ρ_o	density of the cold gas ahead of the spark, gm/cm^3
ϕ	rate of energy loss by radiation, kW/cm^3
ω_n^2	separation constant, equal to x_{on}^2/R_c^2, cm^{-2}

Abstract of Dissertation Presented to the Graduate Council of the University of Florida in Partial Fulfillment of the Requirements for the Degree of Doctor of Philosophy

TWO-DIMENSIONAL MODEL FOR THE SUBSONIC PROPAGATION OF LASER SPARKS

By

Jad Hanna Batteh

August, 1974

Chairman: Dennis R. Keefer
Major Department: Engineering Sciences

The properties of laser sparks are investigated by solving a simplified, two-dimensional energy equation describing the steady state, subsonic propagation of a spark in a channel. The propagation mechanism is assumed to be thermal conduction and thermal radiation is included as an effective optically thin emission. The solution, obtained in closed form, yields both axial and radial temperature profiles, as well as the relationship between the laser beam characteristics, the channel radius and the propagation velocity.

A solution of the radially integrated energy equation is obtained by introducing the radial heat conduction parameter A suggested by Raizer. The parameter is evaluated by means of the solution to the two-dimensional energy equation.

The model is applied to air sparks of .15 cm and .50 cm radius propagating at velocities up to 20 cm/sec under the influence of CO_2 laser radiation. The results indicate a spark length on the order of 1 cm and temperatures near 16,000 ^{o}K. Approximately half the incident laser intensity is absorbed by the spark. Calculation of the radial heat conduction parameter verifies the value of 2.9 used by Raizer for an unbounded spark of .15 cm radius. Furthermore, A is found to depend on the spark radius.

The theory agrees with the experimental results for stationary sparks. However, it fails at predicting the spark properties for propagation velocities of several meters per second. It is postulated that, at these velocities, re-absorption of thermal radiation creates a nonequilibrium layer ahead of the spark front which enhances the absorption of laser radiation and increases the propagation velocity.

CHAPTER I

INTRODUCTION

Interest in the interaction of matter with intense beams of coherent radiation has increased with the development of high power lasers. In particular, extensive research is being devoted to the investigation of discharges maintained by the absorption of laser radiation. These discharges are commonly referred to as laser sparks.

Discharges are in wide demand for technological and diagnostic applications and for laboratory studies of plasma processes. The current methods for the creation and maintenance of discharges are based on the release of electromagnetic energy in a gas. Until recently discharges, which are classified by the frequency of the electromagnetic field, ranged from the direct-current arc discharge to the microwave discharge. Within this frequency range the transfer of electromagnetic energy requires special auxiliary equipment such as electrodes, conductor coils and wave guides. As a result the plasma is confined by boundaries which can erode and introduce contaminants.

The laser spark represents an extension of the frequency range of the generating field to infrared and visible frequencies. The electromagnetic energy is transported by

the laser beam thereby eliminating the need for special equipment. It is possible, therefore, to obtain pure plasmas burning in free space. These characteristics plus the high temperatures attainable in laser sparks extend the possible applications beyond those of lower frequency discharges. For example, a recent study[1] explored the feasibility of using laser sparks to increase the enthalpy of the flowing gas in a hypersonic wind tunnel. These laser-sustained discharges also offer the researcher interested in plasma physics a unique opportunity to study an unconfined plasma in the laboratory.

However, the occurrence of laser sparks is often undesirable. A laser beam of sufficiently high intensity can initiate a spark in a gas or by interaction with solid materials. The intensity of the laser radiation is attenuated in passing through the spark due to the conversion of radiation energy to thermal energy which takes place in the spark. Therefore, the intensity of laser radiation which can be transported to a target is limited by the threshold intensity for the creation of a spark. Exceeding this intensity results in the creation of a laser spark which absorbs a portion of the incident radiation ahead of the target.

Laser sparks generally fall into two categories depending on whether the laser beam ignites the discharge or merely maintains an externally initiated discharge.

Ignition can occur in a gas which is usually transparent to laser radiation if the laser intensity creates sufficient ionization in a region to initiate absorption of the laser energy.[2-4] Due to the high intensities required, ignition has been observed only with the focused output of pulsed lasers. The initial breakdown region quickly develops into a laser spark. Shock waves, driven by the absorption of laser radiation, propagate outward from the hot spark and heat the surrounding areas. In particular, the cold gas ahead of the spark and in the path of the laser beam is ionized and begins to absorb the incident radiation. Thus, a new absorbing layer is created and the spark front propagates in a direction opposite the laser flux due to a mechanism similar to that occuring in the detonation of explosives. Typical spark temperatures are 10^5 to 10^6 ^oK. As the spark propagates, it is observed to expand radially to fill the cone formed by the focused laser beam.

In 1969 Bunkin *et al.*[5] demonstrated for the first time that a laser intensity lower than that required for breakdown could maintain an externally initiated discharge. They found that Nd-glass laser radiation at an intensity of 10^4 kW/cm^2 could maintain an air spark which had been initially ignited by an electrical discharge. This intensity was two orders of magnitude less than that required to initiate breakdown. In this case the incident laser intensity is insufficient for generating a shock wave.

Thermal heat conduction, aided by reabsorption of thermal radiation emitted from the hot spark, is the mechanism by which the cold gas ahead of the spark is ionized and becomes opaque to the incoming laser radiation. The spark propagates subsonically in a direction opposite the laser flux. Typical spark temperatures in the subsonic regime are 10,000 - 25,000 ^{o}K.[5-8]

This mode of propagation suggests the existence of a threshold laser intensity, such that the absorbed laser energy just compensates for the heat conduction and radiation losses, and the spark remains stationary. The existence of a threshold was demonstrated in 1970 by Generalov et al.[6,7] who used a continuous wave (cw) CO_2 laser to maintain a stationary plasma in high pressure argon and xenon gases. Similar experiments have been conducted by Franzen,[9] and recently Smith and Fowler[8] have published data on the threshold intensity of CO_2 laser radiation in atmospheric-pressure air.

The modeling of subsonic laser sparks promotes understanding of the creation and maintenance of these discharges. Unfortunately, only a limited amount of theoretical work has been done. Raizer,[10] using a one-dimensional analysis and introducing a thermal conduction parameter for radial heat losses, derived threshold laser intensities and propagation velocities for sparks in atmospheric-pressure air under the influence of CO_2 and Nd-glass laser radiation. Hall, Maher and Wei,[11]

resorting to analytical approximations for the thermodynamic properties of air, also used a one-dimensional model to obtain the radially averaged spark temperatures and propagation velocity. In both References 10 and 11, thermal conduction was assumed to be the propagation mechanism. A recent one-dimensional study by Jackson and Nielsen[12] has focused on the role of radiation in the subsonic propagation of laser sparks.

The purpose of this investigation is to provide a two-dimensional model for the subsonic propagation of laser sparks by explicitly including the radial heat conduction losses. This allows the calculation of both radial and axial temperature profiles as opposed to temperatures averaged over the radius. Furthermore, the solution is obtained for a spark propagating in a channel of arbitrary radius so that the effect of boundaries on spark propagation can be studied. The model is applied to air sparks at atmospheric pressure under the influence of CO_2 laser radiation.

The propagation mechanism is assumed to be thermal conduction with radiation serving only as an energy loss mechanism. Although the flow velocity is restricted to one dimension, the two-dimensional nature of the temperature field is retained in the analysis. By using simple models for the temperature-dependent properties of the gas, a closed form solution is obtained which yields axial and

radial temperature profiles as well as the dependence of the propagation velocity on channel radius, spark radius and incident laser intensity. The two-dimensional model also offers a method for evaluating the radial heat conduction parameter introduced by Raizer.[10]

CHAPTER II

THEORETICAL DEVELOPMENT

In this analysis the steady state, subsonic propagation of a laser spark in a gas is considered. The ignition process is not considered since its only purpose is to provide free electrons to initiate inverse bremsstrahlung absorption of the laser beam. Therefore, the characteristics of the spark are functions only of the laser-plasma interaction and not of the ignition process.

The model consists of a uniform, monochromatic laser beam, of intensity S_o and constant radius R_L, passing through a channel of radius R_c in which there is an absorbing plasma. Energy is absorbed from the laser beam by the plasma and is transferred to the cold gas through heat conduction. The channel wall is held at a fixed temperature $T = 0$ and is assumed to absorb all radiation incident upon it without re-emission. The spark moves in the channel without distortion with a constant velocity u relative to the cold gas, as shown in Figure 1. Since the flow velocities are subsonic the pressure gradients are small and are neglected in the analysis. Furthermore, the flow kinetic energy is neglected compared to the thermal energy,

since most of the absorbed radiation appears as a temperature increase as opposed to directed fluid motion. Viscous dissipation is also neglected since the loss due to dissipation is less than the losses due to thermal radiation and heat conduction in the region of laser-plasma interaction. For this model the energy and continuity equations referred to a co-ordinate system fixed to the spark are

$$\rho v_x c_p \frac{\partial T}{\partial x} + \rho v_r c_p \frac{\partial T}{\partial r} = \frac{\partial}{\partial x}\left(\lambda \frac{\partial T}{\partial x}\right) + \frac{1}{r}\frac{\partial}{\partial r}\left(r \lambda \frac{\partial T}{\partial r}\right) + S\kappa_\nu - \phi \tag{2.1}$$

$$\frac{\partial}{\partial x}(\rho v_x) + \frac{1}{r}\frac{\partial}{\partial r}(r \rho v_r) = 0 \tag{2.2}$$

In the above equations ρ is the density, T is the temperature, v_x and v_r are the axial and radial velocity components, respectively, $c_p(T)$ is the specific heat capacity, $\lambda(T)$ is the thermal conductivity, S is the intensity of the laser beam, $\kappa_\nu(T)$ is the absorption coefficient at frequency ν and ϕ is the net energy lost by radiation per cm^3 per sec. The density is assumed to be related to the temperature and pressure by the perfect gas law.

In order to solve for both the velocity field and the temperature field, the two momentum equations must be included in the analysis. Clearly, the solution of these four, nonlinear, coupled partial differential equations is

a problem of considerable difficulty unless simplifying assumptions are made. Since the temperature field is of primary interest in this analysis, its two-dimensional nature is retained. On the other hand, the velocity field is simplified by assuming $v_r = 0$ and taking the axial mass flow rate independent of radius. This one-dimensional approximation to the flow field is often used in spark propagation analysis.[10-12] The equations are then uncoupled. In fact, Equation (2.2) reduces to $\rho v_x = \text{const.} = \rho_o u$ where ρ_o is the density far ahead of the spark. Jackson and Nielsen,[12] on the basis of preliminary results, predict little difference between the results obtained using the two-dimensional flow field and the one-dimensional flow field in radiation-dominated propagation. For the model considered here, the error introduced by neglecting the radial deflection of the flow should diminish as the channel radius decreases. Since v_r must vanish at $r = 0$ and $r = R_c$, the channel inhibits the radial velocity.

As a result of the one-dimensional flow approximation, the energy equation reduces to

$$\alpha \frac{\partial \theta}{\partial x} = \frac{\partial^2 \theta}{\partial x^2} + \frac{1}{r} \frac{\partial}{\partial r}\left(r \frac{\partial \theta}{\partial r}\right) + S \dot{\gamma}_\nu - \phi \qquad (2.3)$$

$$\alpha = \frac{\rho_o c_p u}{\lambda}$$

where the thermal flux potential

$$\Theta = \int_{o}^{T} \lambda(T)\, dT$$

has been used to replace T as the dependent variable.

Equation (2.3) can be linearized if suitable approximations are made for the temperature dependence of κ_ν, ϕ, λ and c_p. The first approximation is to assume c_p/λ equal to a constant which reduces α to a constant. Figure 2 shows the variation of this ratio for atmospheric-pressure air plotted from the data of Reference 11. The definite temperature dependance, apparent in the figure, indicates that the assumption is a shortcoming in the theory. However, the assumption is a reasonable first approximation in the temperature range 10,000 - 25,000 ^{o}K which is of greatest interest for subsonic laser sparks. In fact, it will be shown in Chapter VI that this approximation is valid for the velocities considered in this analysis. Although the authors of Reference 11 used analytical approximations for the temperature variations of enthalpy and thermal conductivity, their approximations are equivalent to assuming a constant c_p/λ .

Un-ionized air is transparent to CO_2 laser radiation, which has a wavelength of 10.6 microns. However, absorption can occur by inverse bremsstrahlung (free-free transitions of the electrons) when air becomes ionized.

In that case the free electrons in the presence of scattering centers are accelerated by the electric field of the laser radiation. The electron and heavy-particle temperatures are then equilibrated by elastic collisions.

Although both neutral particles and ions can serve as scattering centers, absorption in the field of neutral particles is important only in a very weakly ionized gas.[13] At typical spark temperatures the ionization is appreciable so that only absorption due to electron-ion collisions is considered.

The inverse bremsstrahlung absorption coefficient for a high-temperature, ionized gas is given by the modified Kramers formula[13]

$$\kappa_\nu = 3.69 \times 10^{8} \frac{Z^2 g N_+ N_e}{T_e^{1/2} \nu^3} \quad cm^{-1} \qquad (2.4)$$

where N_+ is the number density of positive ions with charge Z, N_e is the number density of electrons, T_e is the electron temperature, ν is the radiation frequency and g is the Gaunt factor. In the single ionization temperature range, the absorption coefficient is approximately proportional to $N_e^2/T_e^{\frac{1}{2}}$. Therefore, under equilibrium conditions, κ_ν will exhibit a rapid increase at temperatures where the ionization becomes appreciable. For atmospheric-pressure air this temperature lies in the range 10,000 ^{o}K to 15,000 ^{o}K.[14] In fact, equilibrium calculations[10]

of κ_ν for atmospheric-pressure air show a rapid increase near T = 12,000 ^{o}K.

The absorption coefficient of air for Nd-glass laser radiation, which has a wavelength of 1.06 microns, consists of contributions from both free-free and bound-free electron transitions. It also exhibits a rapid increase at temperatures near 12,000 ^{o}K.[10]

Consequently, the solution domain of the energy equation is divided into two regions separated by the plane x = 0. For $x < 0$ the temperature is sufficiently low that there is negligible absorption of laser radiation, i.e. $\kappa_\nu = 0$. In the region $x > 0$, the absorption coefficient is assumed to be a constant so that

$$S\kappa_\nu = S_o H(R_L - r)\kappa_\nu e^{-\kappa_\nu x}$$

where S_o is the incident laser intensity and $H(R_L - r)$ is the Heaviside step function defined to be unity for $0 \leq r \leq R_L$ and zero for $r > R_L$. The term "spark front" will be used to denote the plane x = 0.

A complete treatment of the emission and re-absorption of thermal radiation would require the solution of a complicated integro-differential equation. It is included in this analysis through a simple phenomenological approximation. In the region $x < 0$, where the temperature is comparatively low and decreases rapidly with increasing

distance from the spark front, the net thermal emission is neglected. In the region $x > 0$, it is included as a simple volumetric loss term given by the linear relationship

$$\phi = m \Theta$$

The constant m is chosen to give values of ϕ which agree with experimentally determined radiation losses for air at temperatures near 15,000 °K.

The analysis of Jackson and Nielsen[12] for large radius sparks suggests that re-absorption of thermal radiation, rather than thermal conduction, is the dominant heating mechanism for the cold gas ahead of the spark. The effect of neglecting this heating, by assuming $\phi = 0$ for $x < 0$, and the role of radiation transport in spark propagation will be discussed in Chapter VI.

As a result of the approximations discussed in the preceding paragraphs, Θ_1 which is the solution for the thermal potential in the region $x < 0$ must satisfy

$$\frac{\partial^2 \Theta_1}{\partial x^2} + \frac{1}{r} \frac{\partial}{\partial r} \left(r \frac{\partial \Theta_1}{\partial r} \right) - \alpha \frac{\partial \Theta_1}{\partial x} = 0 \qquad (2.5)$$

and Θ_2 which is the thermal potential in the region $x > 0$ must satisfy

$$\frac{\partial^2 \theta_2}{\partial x^2} + \frac{1}{r}\frac{\partial}{\partial r}\left(r\frac{\partial \theta_2}{\partial r}\right) - \alpha\frac{\partial \theta_2}{\partial x} - m\theta_2 = -S_0 H(R_L - r)\kappa_\nu e^{-\kappa_\nu x} \tag{2.6}$$

The boundary conditions at $x = \pm\infty$ and at the channel radius R_c are

$$\theta_1(-\infty, r) = \theta_2(\infty, r) = \theta_1(x, R_c) = \theta_2(x, R_c) = 0 \tag{2.7}$$

Since the temperature and the heat flux must be continuous at x = 0, the joining conditions are

$$\theta_1(0, r) = \theta_2(0, r) \tag{2.8}$$

$$\left(\frac{\partial \theta_1}{\partial x}\right)_{x=0} = \left(\frac{\partial \theta_2}{\partial x}\right)_{x=0} \tag{2.9}$$

Equations (2.7) - (2.9), together with the restriction that θ be finite, completely determine the solution. There is, however, one further condition which must be met. Since x = 0 has been defined as the plane where appreciable absorption begins, the temperature at x = 0 as determined from the differential equations must

correspond to the temperature at which the plasma becomes opaque to the laser radiation. This consistency condition is satisfied by requiring the thermal flux potential, averaged over the laser radius at x = 0, to be equal to Θ_i , the value of the potential at the ignition temperature T_i, i.e.

$$\Theta_i = \frac{2}{R_L^2} \int_0^{R_L} r\, \Theta_1(0, r)\, dr \qquad (2.10)$$

This equation results in a relationship between the propagation velocity and the required laser intensity.

CHAPTER III

SOLUTION OF THE EQUATIONS

Equations (2.5) and (2.6) for the thermal potentials can be solved in closed form by the separation of variables technique.

By assuming

$$\Theta_1(x,r) = \sum_n f_n(x)\, g_n(r)$$

the partial differential equation for Θ_1 reduces to a set of ordinary differential equations

$$\frac{d^2 f_n}{dx^2} - \alpha \frac{df_n}{dx} - \beta_n^2 f_n = 0$$

$$\frac{d^2 g_n}{dr^2} + \frac{1}{r}\frac{dg_n}{dr} + \beta_n^2 g_n = 0 \quad , \quad n = 1, 2, \ldots$$

where the β_n^2 are separation constants.

The equation for g_n is Bessel's equation, which has the solution

$$g_n = a_n J_0(\beta_n r) + b_n Y_0(\beta_n r)$$

J_o and Y_o are the zero order Bessel functions of the first and second kind, respectively, and the a_n and b_n are constants. Since $Y_o(0) = \infty$, b_n must be zero for the solution to remain finite on the axis. The radial boundary condition in Equation (2.7) determines the separation constant. For θ_1 to vanish at $r = R_c$, β_n must equal x_{on}/R_c where x_{on} is the n^{th} zero of J_o.

The differential equation for f_n has the solution

$$f_n = c_n e^{\delta_{1n} x} + d_n e^{\delta_{2n} x}$$

where

$$\delta_{1n,2n} = \frac{\alpha}{2}\left[1 \pm \sqrt{1 + \frac{4\beta_n^2}{\alpha^2}}\right]$$

and the c_n and d_n are constants. To satisfy the boundary condition $\theta_1(-\infty, r) = 0$, d_n must be zero.

The solution for θ_1 can, therefore, be written as

$$\theta_1 = \sum_n a_n J_o\left(x_{on}\frac{r}{R_c}\right) e^{\frac{\alpha}{2}(1+\gamma_n)x} \qquad (3.1)$$

$$\gamma_n = \sqrt{1 + \left(\frac{2x_{on}}{\alpha R_c}\right)^2}$$

The constants a_n are determined by the joining conditions.

Equation (2.6) for Θ_2 is a nonhomogeneous, linear partial differential equation. Its solution can be written as

$$\Theta_2 = \Theta_p + \Theta_h$$

where Θ_p is a particular solution, and Θ_h is the solution of the associated homogeneous equation

$$\frac{\partial^2 \Theta_h}{\partial x^2} + \frac{1}{r}\frac{\partial}{\partial r}\left(r \frac{\partial \Theta_h}{\partial r}\right) - \alpha \frac{\partial \Theta_h}{\partial x} - m\Theta_h = 0 \tag{3.2}$$

A particular solution of Equation (2.6) which satisfies the boundary conditions at $r = R_c$ and $x = \infty$ is

$$\Theta_p = e^{-\gamma_\nu x} \sum_n b_n J_o\left(x_{on}\frac{r}{R_c}\right) \tag{3.3}$$

where the b_n are constants. Substituting Equation (3.3) into Equation (2.6) yields

$$\sum_n t_n J_o\left(x_{on}\frac{r}{R_c}\right) = S_o \gamma_\nu H(R_L - r)$$

$$t_n = \left[\left(\frac{x_{on}}{R_c}\right)^2 - \gamma_\nu(\gamma_\nu + \alpha) + m\right] b_n \tag{3.4}$$

Since the $J_o(x_{on}r/R_c)$ form a complete, orthogonal set in the range $0 \leq r \leq R_c$, they can be used to form a unique series expansion of any function of r in that interval. In particular, the function $S_o \kappa_\nu H(R_L - r)$ can be expanded in terms of an infinite series. Therefore, for Equation (3.4) to be valid, the t_n must be the coefficients of such a series expansion. The coefficients can be found by using the orthogonality property[15]

$$\int_0^{R_c} r\, J_o\left(x_{on}\frac{r}{R_c}\right) J_o\left(x_{om}\frac{r}{R_c}\right) dr = \frac{R_c^2}{2} J_1^2(x_{on})\delta_{nm}$$

where δ_{nm} is the Kronecker delta and J_1 is the first order Bessel function of the first kind. Multiplying Equation (3.4) by $rJ_o(x_{om}r/R_c)$, integrating from 0 to R_c and applying the orthogonality condition gives

$$t_n = \frac{2\kappa_\nu S_o}{R_c^2 J_1^2(x_{on})} \int_0^{R_L} r\, J_o\left(x_{on}\frac{r}{R_c}\right) dr$$

The value of the integral, obtained with the aid of Equation (11.3.20) of Reference 15, is $R_c R_L J_1(x_{on}R_L/R_c)/x_{on}$. The resulting equation for the constants b_n of the particular solution is

$$b_n = \frac{2\gamma_\nu S_0 R_L J_1\left(x_{on}\frac{R_L}{R_c}\right)}{x_{on} R_c J_1^2(x_{on})\left[\left(\frac{x_{on}}{R_c}\right)^2 - \gamma_\nu(\gamma_\nu + \alpha) + m\right]}$$

The solution of the homogeneous equation for θ_h is assumed to have the form

$$\theta_h(x,r) = \sum_n F_n(x)\, G_n(r)$$

Substitution into Equation (3.2) results in the set of ordinary differential equations

$$\frac{d^2F_n}{dx^2} - \alpha\frac{dF_n}{dx} - (\omega_n^2 + m)F_n = 0$$

$$\frac{d^2G_n}{dr^2} + \frac{1}{r}\frac{dG_n}{dr} + \omega_n^2 G_n = 0 \quad , \quad n = 1, 2, \cdots$$

where the ω_n^2 are separation constants. The solutions of these equations are obtained in a manner analagous to the procedure used for θ_1. Imposing the boundary conditions $F_n(\infty) = 0$ and $G_n(R_c) = 0$ results in

$$\theta_h = \sum_n c_n J_0\left(x_{on}\frac{r}{R_c}\right) e^{\frac{\alpha}{2}(1-\gamma_n')x}$$

$$\gamma_n' = \sqrt{1 + \frac{4}{\alpha^2}\left[\left(\frac{x_{on}}{R_c}\right)^2 + m\right]}$$

where the c_n are constants to be determined by the joining conditions.

Thus, the solution for Θ_2 is given by

$$\Theta_2(x,r) = e^{-\kappa_\nu x} \sum_n b_n J_0\left(x_{on}\frac{r}{R_c}\right) + \sum_n c_n J_0\left(x_{on}\frac{r}{R_c}\right) e^{\frac{\alpha}{2}(1-\gamma_n')x} \tag{3.5}$$

Imposing the joining conditions given in Equations (2.8) and (2.9) results in a set of algebraic equations for the a_n and c_n. Solution of these equations yields the following for Θ_1 and Θ_2 :

$$\Theta_1 = 8\kappa_\nu S_o \frac{R_L}{R_c} \sum_n A_n J_0\left(x_{on}\frac{r}{R_c}\right) e^{\frac{\alpha}{2}(1+\gamma_n)x} \tag{3.6}$$

$$\Theta_2 = 8\kappa_\nu S_o \frac{R_L}{R_c}\left[e^{-\kappa_\nu x}\sum_n B_n J_0\left(x_{on}\frac{r}{R_c}\right) - \sum_n C_n J_0\left(x_{on}\frac{r}{R_c}\right) e^{\frac{\alpha}{2}(1-\gamma_n')x}\right] \tag{3.7}$$

where the coefficients are given by

$$A_n = \frac{J_1\left(x_{on}\frac{R_L}{R_c}\right)}{\alpha(\gamma_n + \gamma_n')\, x_{on}\, J_1^2(x_{on})\left[\alpha(\gamma_n'+1) + 2\kappa_\nu\right]} \tag{3.8}$$

$$B_n = \frac{\alpha(\gamma_n + \gamma_n')}{\alpha(\gamma_n' - 1) - 2\kappa_\nu}\, A_n \tag{3.9}$$

$$C_n = \frac{\alpha(1 + \gamma_n) + 2\kappa_\nu}{\alpha(\gamma_n' - 1) - 2\kappa_\nu}\, A_n \tag{3.10}$$

The relationship between the propagation velocity and the laser intensity is obtained by substituting θ_1 from Equation (3.6) into Equation (2.10). The resulting equation is

$$\theta_i = 16\,\kappa_\nu\, S_o \sum_n \frac{A_n}{x_{on}}\, J_1\left(x_{on}\frac{R_L}{R_c}\right) \tag{3.11}$$

Since the A_n are functions of α, the propagation velocity is contained in the summation. Therefore, the most convenient way to evaluate Equation (3.11) is to choose a value of u and solve for S_o. Equations (3.6) and (3.7) can then be evaluated for θ_1 and θ_2.

Equations (3.6) - (3.11) are valid only if each infinite series converges uniformly in the interval

$-\infty \leq x \leq \infty$ and $0 \leq r \leq R_c$. A proof of the uniform convergence of these series is given in Appendix I.

The length of the spark d can be defined as the co-ordinate x where the temperature averaged over the laser radius falls below the ignition temperature T_i. Although the model does not terminate absorption of the laser radiation at x = d, the absorption of a real spark decreases rapidly for $x > d$ due to the rapid decrease in the degree of ionization. Therefore, the spark length is useful in approximating the power absorbed by the spark. Consistent with the exponential approximation for the absorption of laser radiation,

$$\frac{P_A}{P_o} = 1 - e^{-\kappa_\nu d} \tag{3.12}$$

where P_A is the power absorbed by the spark and P_o is the incident power.

CHAPTER IV

SIMPLIFIED ONE-DIMENSIONAL ANALYSIS

Although the solution in Equations (3.6) - (3.10) is straightforward, it is cumbersome due to the summation. In this chapter the equations are reduced to one dimension by introducing a radial heat conduction parameter. The parameter is in the form of an infinite series, but the spark properties are described by simple equations.

If Equations (2.5) and (2.6) are averaged over the laser radius, the resulting equations are

$$\frac{d^2\bar{\theta}_1}{dx^2} - \alpha\frac{d\bar{\theta}_1}{dx} - \frac{A\,\bar{\theta}_1}{R_L^2} = 0 \quad , \quad x < 0 \tag{4.1}$$

$$\frac{d^2\bar{\theta}_2}{dx^2} - \alpha\frac{d\bar{\theta}_2}{dx} - \left(m + \frac{A}{R_L^2}\right)\bar{\theta}_2 + S_0\,\gamma_\nu\, e^{-\gamma_\nu x} = 0 \quad , \quad x > 0 \tag{4.2}$$

where

$$\bar{\theta}(x) = \frac{2}{R_L^2}\int_0^{R_L} r\,\theta(x,r)\,dr$$

In Equations (4.1) and (4.2), the radial heat conduction term has been simplified, as suggested by Raizer,[10] by setting

$$\frac{2}{R_L}\left(\frac{\partial \theta}{\partial r}\right)_{r=R_L} = -\frac{A\,\bar{\theta}}{R_L^2} \tag{4.3}$$

The parameter A is assumed to be independent of x and r but it is a function of spark and channel properties.

For the one-dimensional equations, the boundary conditions are

$$\bar{\theta}_1(-\infty) = \bar{\theta}_2(\infty) = 0$$

The joining conditions are given by

$$\bar{\theta}_1(0) = \bar{\theta}_2(0) = \theta_i$$

$$\left(\frac{d\bar{\theta}_1}{dx}\right)_{x=0} = \left(\frac{d\bar{\theta}_2}{dx}\right)_{x=0}$$

The solutions of Equations (4.1) and (4.2) subject to these conditions are

$$\bar{\theta}_1(x) = \theta_i \; e^{\frac{\alpha}{2}(1+\gamma)x} \tag{4.4}$$

$$\bar{\theta}_2(x) = \theta_i \; e^{-\kappa_\nu (x-d)} + \theta_i \left(1 - e^{\kappa_\nu d}\right) e^{\frac{\alpha}{2}(1-\gamma')x} \tag{4.5}$$

where

$$\gamma = \sqrt{1 + \frac{4A}{\alpha^2 R_L^2}} \tag{4.6}$$

$$\gamma' = \sqrt{1 + \frac{4}{\alpha^2 R_L^2}(mR_L^2 + A)} \tag{4.7}$$

$$d = \frac{1}{\kappa_\nu} \ln\left[\frac{\alpha(\gamma + \gamma')}{\alpha(\gamma' - 1) - 2\kappa_\nu}\right] \tag{4.8}$$

The relationship between the propagation velocity and the incident laser intensity is given by

$$S_o = \frac{\theta_i}{4\kappa_\nu}\,\alpha(\gamma + \gamma')\left[\alpha(\gamma' + 1) + 2\kappa_\nu\right] \tag{4.9}$$

If the losses due to radial conduction are much greater than the radiation losses, i.e. $A >> mR_L^2$, and if the absorption coefficient satisfies the relationship $2\kappa_\nu << \alpha(\gamma' + 1)$, then Equation (4.9) reduces to

$$S_o = \frac{\theta_i}{2\kappa_\nu}\,\alpha^2\gamma(\gamma + 1) \tag{4.10}$$

Raizer,[10] neglecting thermal radiation losses and the attenuation of the incident laser beam, obtained

Equation (4.10) in his one-dimensional analysis. For large propagation velocities, γ and γ' both approach unity, if the variation of A with u is neglected. Then Raizer's result that the laser intensity is proportional to u^2 at large velocities is obtained.

For values of x greater than the point of maximum temperature for CO_2 laser radiation, $\bar{\theta}_2$ can be approximated by

$$\bar{\theta}_2 \approx \theta_i \; e^{-\varkappa_\nu (x - d)}$$

so that d is the length of the spark.

By setting the derivative of $\bar{\theta}_2$ in Equation (4.5) equal to zero, the location of the maximum temperature is found to be

$$x_m = \frac{2}{\alpha(\gamma' - 1) - 2\varkappa_\nu} \ln \left[\frac{\alpha(\gamma' - 1)\left(1 - e^{-\varkappa_\nu d}\right)}{2\varkappa_\nu} \right]$$

Raizer[10] uses a highly empirical method for calculating the thermal conduction parameter. If the axial variations are neglected within a cylinder of radius R_L with strongly cooled walls, the thermal potential will vary approximately as $J_o(x_{01} r/R_L)$. When substituted into Equation (4.3), this distribution results in the value $A = x_{01}^2 = 5.8$. To take into account the fact that the temperature is still quite high at $r = R_L$, Raizer reduces this value by $\frac{1}{2}$ and uses an effective A = 2.9.

A more accurate determination of this parameter can be obtained from the two-dimensional solution presented in Chapter III. By using Equation (3.6) to calculate $\bar{\theta}$ and the radial derivative, substituting into Equation (4.3) and evaluating at x = 0 the following equation for A is obtained:

$$A = \left(\frac{R_L}{R_c}\right)^2 \sum_n x_{on}^2 T_n \left(\sum_n T_n\right)^{-1} \qquad (4.11)$$

where $T_n = (A_n/x_{on})J_1(x_{on}R_L/R_c)$. The convergence of the infinite series is demonstrated in Appendix I.

CHAPTER V

EXAMPLE CALCULATIONS

The equations derived in Chapters III and IV have been used to study the properties of sparks maintained in atmospheric-pressure air by CO_2 laser radiation.

The variation of the thermal potential with temperature, obtained from the data of Reference 11, is shown in Figure 3. A value of .15 kW/cm was used for the value of the thermal potential at ignition. This value corresponds to the ignition temperature T_1 = 12,000 ^{o}K suggested by Raizer.[10]

The absorption coefficient γ_ν for CO_2 laser radiation in air increases rapidly for temperatures greater than 12,000 ^{o}K, due to the rapidly increasing degree of ionization.[10] It reaches a maximum value of approximately .85 cm^{-1} at T = 17,000 ^{o}K and decreases to a minimum of .38 cm^{-1} at T = 24,000 ^{o}K. This behavior can be understood by considering the formula for γ_ν given in Equation (2.4) Beyond 17,000 ^{o}K, first ionization is essentially complete. The electron density approaches a plateau while the temperature T_e continues to increase. Therefore, γ_ν decreases. For temperatures greater than 24,000 ^{o}K, the electron density again increases rapidly due to the

ionization of singly charged ions. Consequently, the absorption coefficient increases for temperatures greater than 24,000 ^{o}K. The value $\chi_{\nu} = .74$ cm^{-1} was used in the calculations for $x > 0$. It corresponds to an average value for the temperature range 15,000 ^{o}K to 20,000 ^{o}K, which are typical values for the temperature in the spark core.

The ratio c_p/λ was set equal to 425 cm sec/gm. From Figure 1 this corresponds to a mean value in the temperature range 10,000 ^{o}K to 20,000 ^{o}K. The upstream density was taken as $\rho_o = 1.3 \times 10^{-3}$ gm/cm^3.

The thermal emission parameter m was assumed to be 175 cm^{-2}. The resulting losses are 44 kW/cm^3 and 67 kW/cm^3 for T = 15,000 ^{o}K and 20,000 ^{o}K, respectively. Raizer's calculations[10] indicate losses which vary from 48 kW/cm^3 to 60 kW/cm^3 over the same interval, with the maximum occurring at 18,000 ^{o}K. However, he uses only half of this emission in his calculations since he assumes half of the radiation is re-absorbed in the cold gas ahead of the spark and not really lost. The experimental and theoretical work of Hermann and Schade[16,17] on wall-stabilized nitrogen arcs at atmospheric pressure indicate radiation losses of 50 kW/cm^3 at 20,000 ^{o}K. Therefore, the linear approximation with m = 175 cm^{-2} adequately represents the losses in the hot zone of the air spark.

With these values of the parameters, Equations (3.6) - (3.11) were used to study the propagation velocities, threshold intensities and temperature profiles for air sparks of radius .15 and .50 cm. Calculations were carried out for propagation velocities from 0 to 20 cm/sec. The channel radius was varied from $R_c = R_L$ to $R_c = 2R_L$. A computer program was written to evaluate the series. It was found that twenty terms were sufficient to insure convergence for the range of parameters studied.

The variation of laser intensity with channel radius for several propagation velocities is shown in Figure 4. For a spark of .15 cm radius, a decrease in channel radius results in a significant increase in the laser intensity required to maintain the spark. The presence of the channel boundary constricts the radial temperature profile. Therefore, the radial heat conduction loss from the spark is increased as R_c decreases, and a higher laser intensity is required to overcome the increased losses.

The energy loss per unit volume due to thermal conduction in the radial direction is proportional to R_L^{-2}, whereas the loss per unit volume due to optically thin radiation is independent of radius. Therefore, thermal radiation becomes the dominant loss mechanism for large radius sparks. In that case the presence of a boundary should have little effect on spark propagation. This is demonstrated in Figure 4, which shows that the required

intensity for R_L = .50 cm is nearly independent of channel radius.

Figures 5 and 6 show the isotherms, calculated from Equations (3.6) - (3.11), for a spark of .15 cm radius in a channel with radius $R_c = 1.25\ R_L$. Figure 5 depicts the threshold isotherms, and Figure 6 shows the isotherms for u = 20 cm/sec. The intense core and elongated structure agrees with the qualitative description of laser sparks given by Smith and Fowler.[8]

Figures 7 and 8 show the isotherms for a spark of .50 cm radius in a channel with radius $R_c = 1.25\ R_L$. The isotherms of Figure 7 correspond to the threshold case while those of Figure 8 correspond to a propagation velocity of 20 cm/sec. The blunter isotherms, as compared to the isotherms of Figures 5 and 6, are due to the decreasing importance of radial heat conduction.

The plots of the isotherms show a rapid increase in temperature at the spark front followed by a slow decrease. The increase is due to the sudden deposition of energy, as a result of the rapid increase in the absorption coefficient at T = 12,000 ^{o}K. The slow decline in temperature for the regions beyond the temperature maximum is a consequence of the small absorption coefficient for CO_2 laser radiation. The absorption length for CO_2 laser radiation in air is $\ell_\nu = \kappa_\nu^{-1} = 1.4$ cm. Therefore, there is little attenuation of the beam when it traverses

distances on the order of $.10\ \ell_\nu$. As a result points separated by this distance absorb almost the same energy from the laser beam.

Figures 5 - 8 show that the isotherms for propagating sparks are blunter at the spark front when compared to the isotherms for stationary sparks. This is a result of convective cooling. In the regions near x = 0, the convective cooling decreases with radius since $\partial\theta/\partial x$ decreases with r. This implies that the hotter regions near the axis are cooled more strongly than the outer, cooler regions. Thus, convection tends to decrease the radial variation of temperature near the spark front.

Representative values of the physical properties of laser sparks, as calculated from Equations (3.6) - (3.12), are given in Table I. The symbol $\bar{\theta}_m$ denotes the maximum value of the radially averaged potentials, and $\bar{T}_m$ is the corresponding temperature. For the cases considered in this analysis the spark is on the order of a centimeter in length with average temperatures near 16,000 ^{o}K. Approximately half the incident laser intensity is absorbed by the spark. The higher intensity required to maintain a propagating spark, as opposed to a stationary spark, results in an increase in both the temperature and the spark length.

The variation of the thermal conduction parameter A, calculated for threshold conditions, with channel radius

is shown in Figure 9. The results indicate that A = 2.9 for a spark of .15 cm radius in a channel of .30 cm radius.

As discussed in Chapter IV, Raizer[10] obtained this same value by an approximate calculation. The agreement is only coincidental since his calculation indicates A is independent of R_L. In fact, the authors of Reference 11 use A = 2.9 for sparks with R_L varying from .028 cm to 1.67 cm. Figure 9 shows, however, that A is a function of laser radius. For $R_c/R_L = 2$, the value of A for a spark of .50 cm radius is nearly twice the value for a spark of .15 cm radius.

Calculations of threshold laser intensities by substituting A from Figure 9 into Equation (4.9) gave excellent agreement with the results of the two-dimensional analysis. Although A was found to vary with propagation velocity, an error of no more than 5% was incurred in using the value of A at threshold to calculate S_o for propagation velocities up to 20 cm/sec,

The one-dimensional solution can be used to study the relative importance of each loss process in subsonic spark propagation. Dividing each loss term in Equation (4.2) by the volumetric energy absorption $S_o \gamma_\nu \exp(-\gamma_\nu x)$ results in nondimensional parameters for the losses due to axial heat conduction, convection, thermal radiation and radial heat conduction.

The variations of these nondimensional parameters with axial distance are shown in Figures 10 and 11 for R_L = .15 cm, R_c = 1.25 R_L and propagation velocities of 0 and 20 cm/sec. These are the same conditions used to obtain the isotherms in Figures 5 and 6. The axial location of the temperature maximum x_m has been used to nondimensionalize the axial distance from the spark front. The values of x_m are .132 and .176 cm for u = 0 and 20 cm/sec, respectively.

Figures 10 and 11 show that the losses due to radial heat conduction and to thermal radiation are approximately equal for R_L = .15 cm. For $x > x_m$ they are the dominant loss mechanisms. Axial heat conduction is important only near x = 0, where the rapid increase in temperature occurs. Likewise, axial convection losses, for the velocities considered in this analysis, are significant only near the spark front, where $\partial\theta/\partial x$ is large. Beyond x_m, axial convection becomes an energy source due to the change in sign of the axial gradient of the temperature.

Figures 12 and 13 show the variations of the nondimensional losses for a spark of radius .50 cm propagating at velocities of 0 and 20 cm/sec in a channel with R_c = 1.25 R_L. These are the conditions for which the isotherms in Figures 7 and 8 were plotted. As in Figures 10 and 11, the axial location of the temperature

maximum has been used to nondimensionalize the axial distance. For Figures 12 and 13, x_m equals .129 cm and .231 cm, respectively.

Figures 12 and 13 illustrate the dominant role of thermal radiation in the dissipation of energy for sparks of large radius. Radial heat conduction accounts for only 10% of the energy loss. Again, axial heat conduction and convection, for the velocities considered here, are important only near the spark front.

It is apparent from Figures 10 - 13 that the laser intensity for a propagating spark must exceed the threshold intensity so that the additional loss due to convection at the spark front can be overcome. However, near the temperature maximum convective losses are negligible so that the increased laser intensity results in a higher maximum temperature for a propagating spark than for a stationary one. Beyond x_m, convection actually is a heating term. The spark length increases with propagation velocity due to this additional source of energy and due to the increase of laser intensity with propagation velocity. These results are illustrated in Figures 5 - 8 and in Table I.

CHAPTER VI

DISCUSSION OF RESULTS

Previous theoretical studies of laser spark phenomena have not probed the effect of a channel boundary on subsonic spark propagation. In fact, aside from models based on Raizer's one-dimensional approximation, only the spherically symmetric case has been considered.[18] Consequently, the conclusions drawn from this analysis cannot be compared with previous theoretical results.

The technology of cw CO_2 lasers has only recently attained the power levels required to maintain subsonic laser sparks in air. As a result, experimental investigations are scarce, and they have not focused on spark propagation in channels. However, the predictions for $R_c/R_L = 2$ can be compared with the results of experiments on unbounded sparks since the channel boundary is far enough from the spark that its influence is negligible. A spark with $R_c/R_L = 2$ will be denoted a "free" spark.

Fowler *et al.*,[19] using a focused CO_2 laser beam in atmospheric-pressure air, studied threshold intensities and propagation velocities. They also determined the spatial variation of temperature and electron number density by a laser interferometric technique. Their

results indicate a threshold intensity near 100 kW/cm^2 for a .15 cm radius spark. This value agrees well with the value of 106 kW/cm^2 obtained from Figure 4 for a free spark of .15 cm radius.

The isotherms of Fowler et al.[19] for an incident power of 6.2 kW can be compared with the isotherms of Figure 5, which correspond to an incident power of 7.8 kW. The experimental results indicate an intense core, with a maximum temperature of 17,000 ^{o}K, and an elongated structure. For example, the maximum radial extent of the 14,000 ^{o}K isotherm is .10 cm and its length is .70 cm. From Figure 5, the values of the radial extent and length of the 14,000 ^{o}K isotherm are .12 cm and .80 cm, respectively. The authors of Reference 19 found that thermal radiation was the dominant loss mechanism for $R_L > .25$ cm, in agreement with the results of Chapter V.

Recently Keefer et al.[20] studied the threshold properties of laser sparks in air. They estimated the threshold intensity to be 120 kW/cm^2 for $R_L = .10$ cm. Using spectroscopic techniques, they found isotherms with a spatial variation similar to the variation reported by Fowler et al.[19] The maximum radial extent and length of the 14,000 ^{o}K isotherm were found to be .15 cm and 1.14 cm, respectively.

In light of the available experimental results, the model appears capable of predicting the threshold properties

of small radius sparks. It is worthwhile to consider the simplifying assumptions and the limitations they impose on the use of the model.

The temperature dependance of c_p/λ was neglected in the analysis. This approximation has no effect on threshold calculations (u = 0) since the ratio appears only in the convective loss term. For the propagation velocities considered in this analysis, convection is significant only near the spark front, as discussed in Chapter V. There the temperatures are not much different from the ignition temperature T_i. Therefore, c_p/λ can be considered constant at a value typical of temperatures near 12,000 ^{o}K.

The absorption coefficient γ_ν was assumed to be zero for $x < 0$ and a constant equal to .74 cm^{-1} for $x > 0$. The two regions are separated by the plane x = 0 where the temperature averaged over the laser radius equals the ignition temperature T_i. Actually the absorption coefficient has a maximum value of approximately .85 cm^{-1} at T = 17,000 ^{o}K and decreases to .60 cm^{-1} at 20,000 ^{o}K. Therefore, temperatures in excess of 17,000 ^{o}K are more difficult to achieve than the model supposes.

Raizer[10] has calculated maximum temperatures for the one-dimensional case taking into account the variation of γ_ν with temperature. His analysis shows that the maximum temperature increases with propagation velocity

and that these temperatures do exceed 17,000 ^{o}K. These results support the temperature variation with velocity indicated in Table I and in Figures 5 - 8.

Hall et al.[11] compared the results for a two-step variation of κ_ν with a one-step model and concluded that the one-step model was a good approximation. Their solutions also indicate an increase in temperature associated with an increase in propagation velocity.

Therefore, the step-function formulation of κ_ν used in this analysis should not introduce appreciable error into the calculations of S_o, the required laser intensity, or $\bar{T}_m$, the maximum of the radially averaged temperatures. However, an analysis including the actual temperature variation of κ_ν would cause some suppression of temperatures greater than 17,000 ^{o}K. For example, there would be a slight decrease in the area within the 20,000 ^{o}K isotherm shown in Figure 6.

For values of $x > d$ the temperature falls below 12,000 ^{o}K and κ_ν decreases rapidly. Since the model retains the value of .74 cm^{-1}, the temperatures predicted by the model in that region exceed those which actually occur. The error introduced by this approximation is not severe since the spark attenuates the laser intensity to approximately half its initial value.

The analysis treats the transport of thermal radiation in an approximate manner. The assumption that the radiation

transport can be represented by an optically thin emission proportional to the thermal flux potential is an oversimplification. Actually, the net energy loss due to thermal radiation can only be found by solving the radiative transfer and energy equations simultaneously. As discussed in Chapter V, the role of radiation increases with spark radius. As a consequence, sparks of large radius may require a more careful treatment of the radiation transport.

The analysis presented here has been limited to propagation velocities of 20 cm/sec or less. However, experiments[5,8,19] indicate that the combustion front velocities can exceed several meters per second. The propagation of sparks at such high velocities by thermal conduction alone leads to excessively high temperatures. For example, the solution of Equations (3.6) - (3.11) for a free spark of radius .50 cm propagating at 1 m/sec yields a required laser intensity of 740 kW/cm^2. This intensity results in a value of $\bar{T}_m$ exceeding 40,000 ^{o}K, which is a factor of two greater than experiments indicate.[5,8,19]

Due to the thermal expansion of the spark, the velocity in the laboratory frame can exceed u which is the velocity measured relative to the cold gas ahead of the spark.[5,10,18] The magnitude of the difference can only be obtained by solving the full two-dimensional flow equations. It is doubtful, however, that thermal expansion could account for the large discrepancy.

The discrepancy between observed and predicted velocities has led to a closer examination of the role of thermal radiation in spark propagation. Several researchers[10-12,18] have noted that radiation emitted by the hot spark can be re-absorbed by the cold gas ahead of the spark. Jackson and Nielsen[12] have shown that, for large radius sparks, heating of the cold gas by re-absorption can far exceed the heating due to thermal conduction. Their results predict propagation velocities of several meters per second with temperatures $\bar{T}_m$ of approximately 20,000 ^{o}K. However, the velocities they obtain are still a factor of five less than the experimental results they use for comparison.

The experiment of Keefer et al.[20] suggests that highly nonequilibrium processes may be occurring in the cooler plasma regions. They found that the dominant radiation in the sheath surrounding the hot plasma core came from the 1^{st} negative system of N_2^+. Furthermore, radiation from the 2^{nd} positive system of N_2, usually present in high-temperature air, was conspicuously absent. The anomalous N_2^+ radiation indicates that nonequilibrium processes, such as photoionization, may be occurring.

This result suggests another explanation for the high propagation velocities. The thermal radiation escaping the plasma core, rather than raising the temperature of the cold gas as a whole as assumed in Reference 12,

could lead instead, through photoionization and inverse bremsstrahlung absorption, to a nonequilibrium region ahead of the spark. A discussion of this phenomenon and its effects on spark propagation is given in Appendix II.

CHAPTER VII

CONCLUSIONS

The two-dimensional energy equation describing spark propagation in a channel has been used to investigate the properties of subsonic laser sparks. The closed-form solution yields both axial and radial temperature profiles, as well as the dependance of the propagation velocity on the incident laser intensity, laser radius and channel radius.

The model was applied to .15 cm and .50 cm radius sparks driven by CO_2 laser radiation at velocities up to 20 cm/sec in atmospheric-pressure air. The results indicate the channel has a significant influence on spark propagation for the .15 cm spark when the channel radius is less than twice the spark radius. For sparks of .50 cm radius, the effect of the channel is negligible.

For the cases considered, the spark length ranges from .34 cm to 1.26 cm. The maximum value of the radially averaged temperature varies from 13,000 ^{o}K to 17,000 ^{o}K. The ratio of the power absorbed by the spark to the incident power ranges from 22% to 61%. For a fixed R_L and R_c, these quantities increase with increasing laser intensity.

For the .15 cm spark, radial heat conduction and thermal radiation losses are approximately equal. However, for the .50 cm spark, radiation is the dominant loss mechanism. In both cases, axial convection and axial heat conduction are significant only near the spark front.

The predicted threshold intensity and isotherm variations for the.15 cm spark agree with the available experimental data. However, the model fails to predict the high propagation velocities experimentally observed. In order to maintain such high velocities, thermal radiation must play a significant role in the heating of the cold gas ahead of the spark.

An equation for the thermal conduction parameter A, introduced by Raizer, has been obtained from the two-dimensional solution. The evaluation of A for a free spark of .15 cm radius confirms the value of 2.9 used by Raizer. Furthermore, A was found to depend on channel and laser radius.

In summary, the two-dimensional model presented in this analysis can be used as a reasonable approximation for the properties of laser sparks at threshold and at low propagation velocities. In those cases, the assumption that thermal radiation serves only as a loss mechanism is adequate. For high propagation velocities, a more careful treatment of the radiation transfer is required.

In spite of the rapidly expanding theoretical and experimental efforts, understanding of subsonic spark phenomena is far from complete. In particular, the observed propagation velocities have eluded a satisfactory explanation. Further analysis in two areas would provide greater insight into the physical processes occurring in subsonic sparks. A detailed study of the radiation transport, including nonequilibrium effects, would provide a more complete knowledge of the propagation mechanism. And a study of the two-dimensional flow field around the spark would lead to a more accurate determination of the role convection plays in the energy balance.

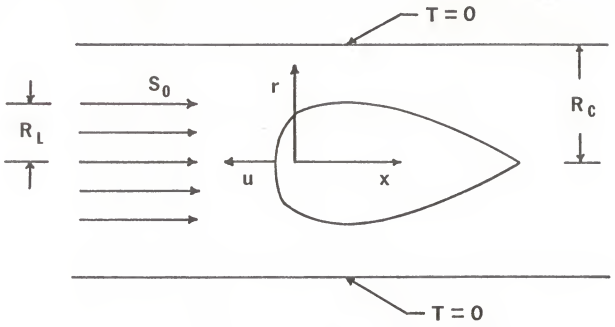

Figure 1. Co-ordinate System for the Steady State Propagation of a Laser Spark in a Channel.

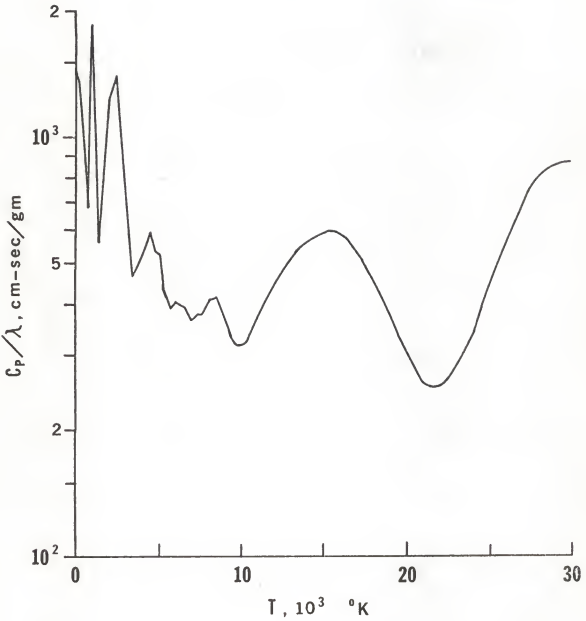

Figure 2. Variation of c_p/λ with Temperature for Atmospheric-pressure Air.

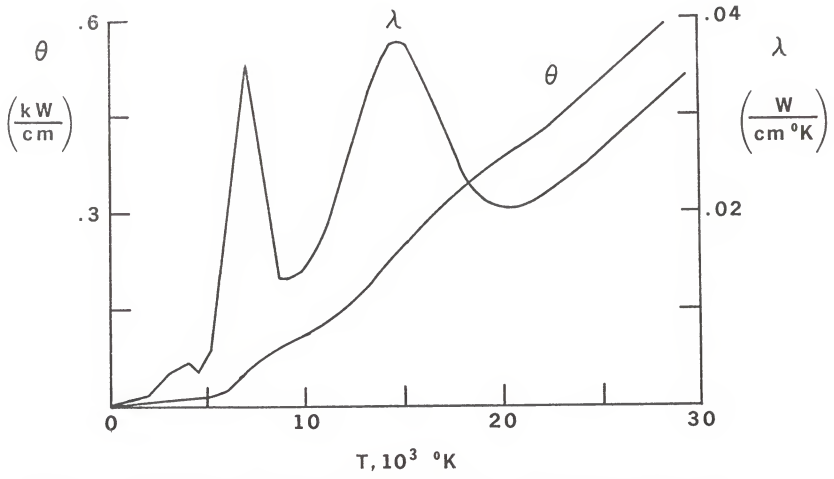

Figure 3. Variation of Thermal Conductivity λ and Thermal Potential θ with Temperature for Atmospheric-pressure Air.

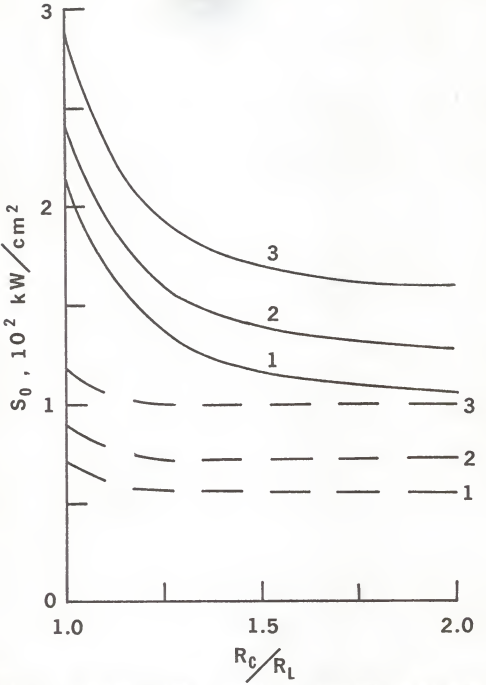

Figure 4. Incident Laser Intensity Required to Maintain a Spark as a Function of Channel Radius. Solid curves are for R_L = .15 cm and broken curves are for R_L = .50 cm. Curves 1, 2 and 3 correspond to velocities of 0, 10 and 20 cm/sec, respectively.

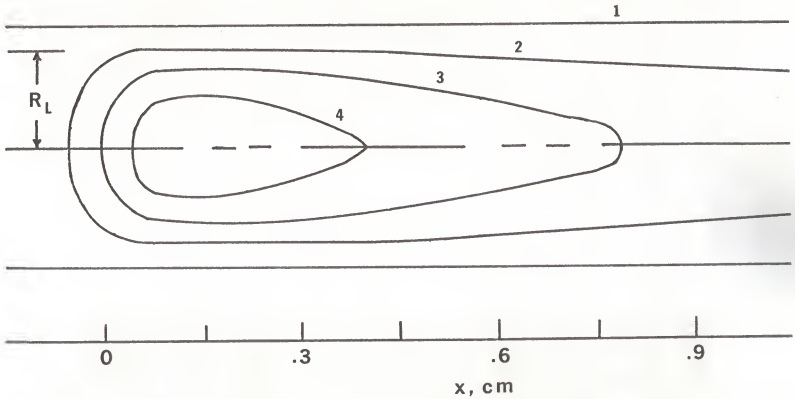

Figure 5. Isotherms for a Spark with R_L = .15 cm, R_c = 1.25 R_L and u = 0. (1) T = 0, (2) T = 10,000 ^oK, (3) T = 14,000 ^oK, (4) T = 16,000 ^oK.

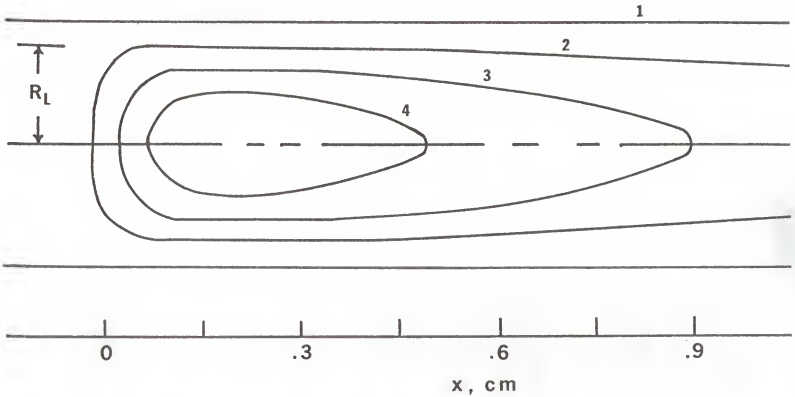

Figure 6. Isotherms for a Spark with R_L = .15 cm, R_c = 1.25 R_L and u = 20 cm/sec. (1) T = 0, (2) T = 12,000 ^oK, (3) T = 16,000 ^oK, (4) T = 20,000 ^oK.

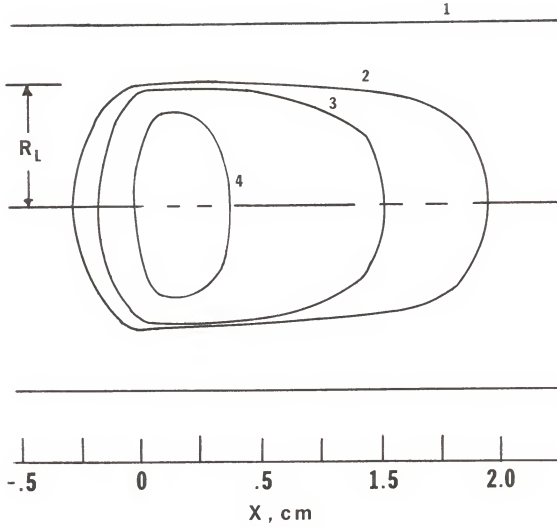

Figure 7. Isotherms for a Spark with R_L = .50 cm, R_c = 1.25 R_L and u = 0. (1) T = 0, (2) T = 8,000 °K, (3) T = 10,000 °K, (4) T = 13,000 °K.

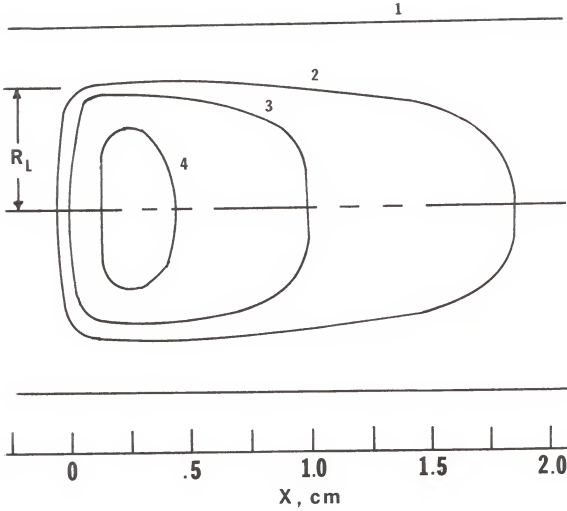

Figure 8. Isotherms for a Spark with R_L = .50 cm, R_c = 1.25 R_L and u = 20 cm/sec. (1) T = 0, (2) T = 10,000 ^oK, (3) T = 14,000 ^oK, (4) T = 17,000 ^oK.

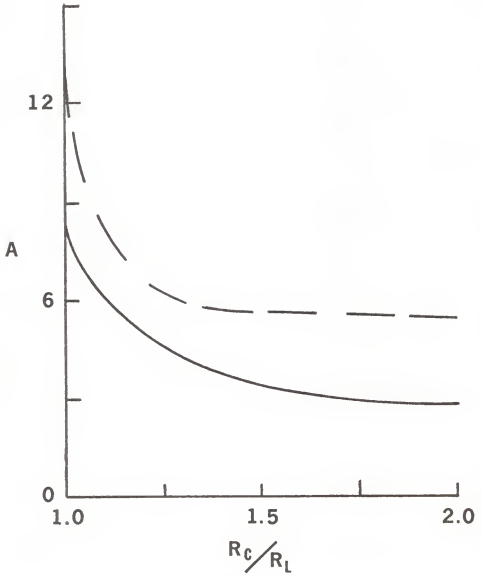

Figure 9. Variation of the Thermal Conduction Parameter with R_c/R_L. Solid curve is for R_L = .15 cm and broken curve is for R_L = .50 cm.

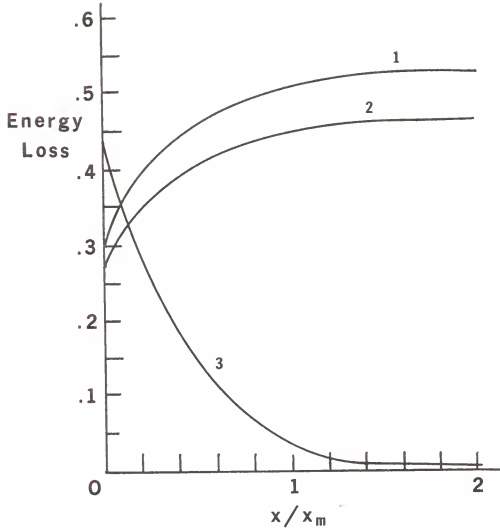

Figure 10. Axial Variation of the Volumetric Energy Loss Terms for R_L = .15 cm, R_c = 1.25 R_L and u = 0. (1) Radial heat conduction, (2) Thermal radiation, (3) Axial heat conduction.

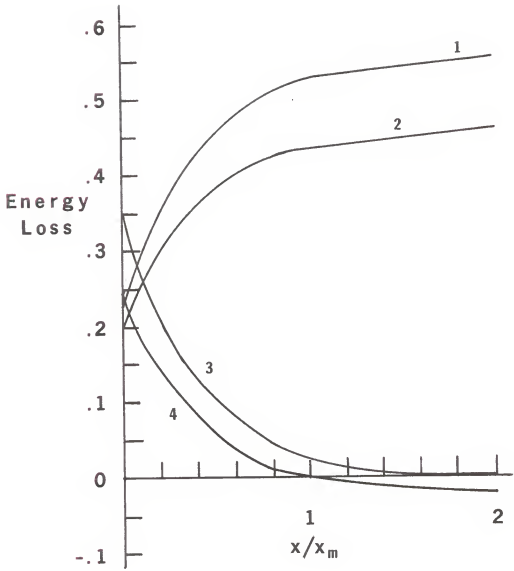

Figure 11. Axial Variation of the Volumetric Energy Loss Terms for R_L = .15 cm, R_c = 1.25 R_L and u = 20 cm/sec. (1) Radial heat conduction, (2) Thermal radiation, (3) Axial heat conduction, (4) Convection.

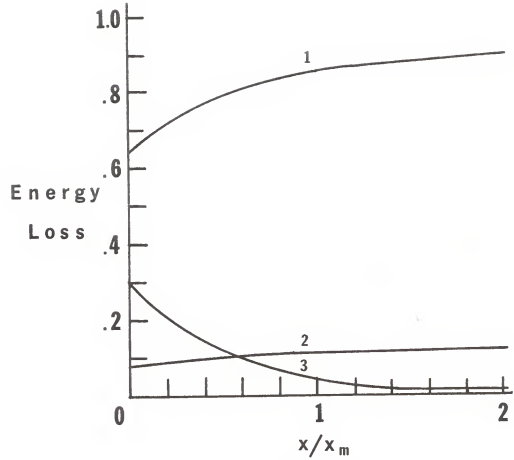

Figure 12. Axial Variation of the Volumetric Energy Loss Terms for R_L = .50 cm, R_c = 1.25 R_L and u = 0. (1) Thermal radiation, (2) Radial heat conduction, (3) Axial heat conduction.

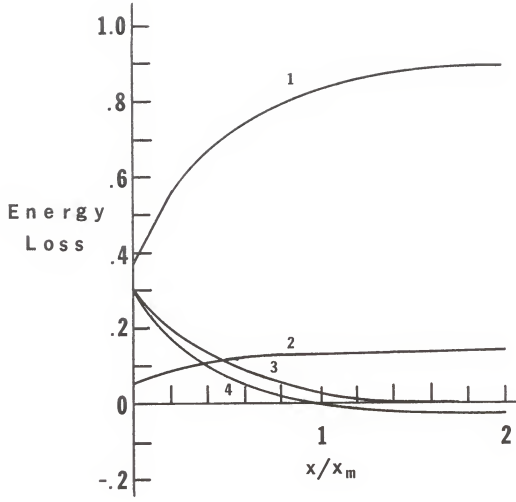

Figure 13. Axial Variation of the Volumetric Energy Loss Terms for R_L = .50 cm, R_c = 1.25 R_L and u = 20 cm/sec. (1) Thermal radiation, (2) Radial heat conduction, (3) Axial heat conduction, (4) Convection.

Table I

Physical Properties of Laser Sparks
of .15 cm and .50 cm Radius

R_c	u	$\bar{\theta}_m$	$\bar{T}_m$	d	P_A/P_o
cm	cm/sec	kW/cm	10^3 °K	cm	
		R_L = .15 cm			
.15	0.	.24	15.	.83	.46
.15	10.	.28	16.	1.02	.53
.15	20.	.32	17.	1.24	.60
.30	0.	.21	14.	.66	.39
.30	10.	.25	15.	.94	.50
.30	20.	.31	17.	1.26	.61
		R_L = .50 cm			
.50	0.	.19	13.5	.50	.31
.50	10.	.23	14.5	.84	.46
.50	20.	.30	16.5	1.26	.61
1.00	0.	.17	13.	.34	.22
1.00	10.	.22	14.	.74	.42
1.00	20.	.29	16.	1.21	.59

APPENDIX I

CONVERGENCE OF THE SERIES SOLUTION

The two-dimensional energy equation describing subsonic spark propagation was solved in Chapter III in terms of infinite series. For the solution to be valid, the series must be shown to converge uniformly for every point (x,r) in the solution domain $-\infty \leq x \leq \infty$, $0 \leq r \leq R_c$.

The following properties of Bessel functions and their zeroes will be used in proving the convergence of the series:[21]

$$\left| J_o(z) \right| \leq 1 \tag{A1.1}$$

$$\left| J_1(z) \right| \leq 1 \tag{A1.2}$$

$$J_1(x_{on}) \neq 0 \tag{A1.3}$$

$$\lim_{n \to \infty} x_{on} = (n - \tfrac{1}{4})\pi \tag{A1.4}$$

$$\lim_{z \to \infty} J_1(z) = .798\, z^{-\frac{1}{2}} \cos(z - 3\pi/4) \tag{A1.5}$$

$$\lim_{n \to \infty} x_{on}\, J_1^{\,2}(x_{on}) = .637 \tag{A1.6}$$

The uniform convergence of a series of function can be proved by the Weierstrass M-Test.[22] It states that the series $\sum_n f_n(x,r)$ converges uniformly in an interval of the variables x and r if $\left| f_n(x,r) \right| \leq M_n$ in that interval and $\sum_n M_n$ converges.

In both Equations (3.6) and (3.7), the exponential term and Bessel function which multiply the A_n, B_n and C_n are bounded, in absolute value, by one. For the series in Equation (3.6), M_n can be taken as

$$M_n = \left[\alpha^2 \gamma_n' \left(\gamma_n + \gamma_n' \right) \chi_{on} J_1^2 \left(\chi_{on} \right) \right]^{-1}$$

since $|A_n| \leq M_n$. From the definitions of γ_n and γ_n' and Equation (A1.4),

$$\lim_{n \to \infty} \gamma_n = \lim_{n \to \infty} \gamma_n' = \frac{2\pi n}{\alpha R_c}$$

Therefore,

$$\lim_{n \to \infty} M_n = Dn^{-2}$$

where D is a positive, finite constant for $R_c < \infty$. Since the series $\sum_n n^{-2}$ converges and since

$$\lim_{n \to \infty} M_n / n^{-2} = D < \infty$$

then $\sum_n M_n$ converges by comparison.[22] Consequently, the infinite series in Equation (3.6) converges uniformly. The convergence of Equation (3.11) follows by comparison with the series $\sum_n A_n$.

At first glance, the two series in Equation (3.7)

appear to have singularities at values of velocity such that

$$\alpha \quad (\gamma_n' - 1) \;=\; 2\,\pi_\nu$$

However, when this condition is satisfied, the exponential factors for the two series are equal. The two series can then be written as one series with coefficients $D_n = B_n + C_n$. When this is done, the singularity disappears.

By the Weierstrass M-Test, the series in Equation (3.7) are uniformly convergent if the series $\sum_n |B_n|$ and $\sum_n |C_n|$ converge. The convergence is easily shown by comparison. Since

$$\lim_{n \to \infty} \; |B_n| \;/\; |A_n| \;=\; 2$$

$$\lim_{n \to \infty} \; |C_n| \;/\; |A_n| \;=\; 1$$

and $\sum_n |A_n|$ converges, then $\sum_n |B_n|$ and $\sum_n |C_n|$ converge.

The infinite series $\sum_n x_{on}^{\,2}\, T_n$ in Equation (4.11) can be shown to converge by comparison with the series $\sum_n n^{-3/2}$. By applying Equations (A1.4) - (A1.6) it can be shown that

$$\lim_{n \to \infty} \; \frac{x_{on}^2\, T_n}{n^{-3/2}} \;=\; \frac{R_c^{\,3}}{8\pi R_L} \lim_{n \to \infty} \; \frac{\cos^2\left(x_{on}\dfrac{R_L}{R_c} - \dfrac{3\pi}{4}\right)}{n^{1/2}}$$

$$= \; 0$$

Therefore, the series $\sum_n x_{on}^{\,2}\, T_n$ converges.

APPENDIX II

EFFECT OF RADIATION ON SUBSONIC SPARKS

It was determined in Chapter VI that spark propagation at velocities of several meters per second by thermal conduction results in temperatures which exceed the experimentally observed temperatures. Therefore, it has been postulated that re-absorption of thermal radiation plays a dominant role in the propagation of laser sparks at high velocities.

Jackson and Nielsen[12] obtained propagation velocities of several meters per second by including radiative transfer in a one-dimensional model. Their solution was based on calculations of the radiative emission and absorption for equilibrium air. The recent results of Keefer et al.[20] suggest, however, that highly nonequilibrium processes are occurring in the cooler plasma regions.

Except for two limiting cases, the solution of the energy equation including radiative transfer poses a problem of considerable difficulty. In the optically thick limit, where the mean free path of the thermal radiation l_ν is much less than some characteristic dimension of the spark L, the radiative energy flux can be written as $\lambda_r \vec{\nabla} T$, where λ_r (T) is the radiative analogue of the thermal conductivity.[23] In that case, the effect of radiative transport is merely an

increase in the thermal conduction coefficient. In the optically thin limit, where $\ell_\nu >> L$, the plasma acts as a volume radiator, and the rate of energy loss per unit volume can be written as a function of temperature.[23] Both limiting cases are valid only where local thermodynamic equilibrium exists.

The model described in Chapter II assumes that radiation can be treated as an effective, optically thin emission. This assumption is adequate for small radius sparks propagating at low velocities. In that case, energy transport by thermal radiation is no greater than energy transport by thermal conduction.

For laser sparks in which radiation dominates the energy transport, the radiative transfer, unfortunately, is neither optically thick nor optically thin. The radiation escaping the hot plasma core lies in the vacuum ultraviolet (vuv).[12] In the core region, where there is a high degree of ionization, the plasma is optically thin to vuv radiation. However, in the cooler regions this radiation is strongly absorbed by the neutral species.

Jackson and Nielsen[12] found that most of the emission from the plasma core lies in the energy range from 14.5 to 20 ev, due mainly to electron recombination with N^+ and O^+ ions. Photons within that range possess energy exceeding the ionization potentials E_i of the neutral species of air, E_i being 15.6 ev, 12.1 ev, 14.5 ev and 13.6 ev for N_2, O_2, N and O, respectively.[24] The photoionization cross sections

for photons whose energy exceeds E_1 are high. For N_2 and O_2 these cross sections are on the order of 20 Mb, where a megabarn (Mb) equals 10^{-18} cm^2. For N and O the cross sections are approximately 8 Mb.[24-26]

The absorption coefficient for the photons equals the sum, over the absorbing species present, of the product of the cross section for photoionization and the number density. Equilibrium, atmospheric-pressure air at 12,000 ^oK is composed primarily of neutral nitrogen and oxygen atoms.[14] The combined neutral atom densities are on the order of 5×10^{17} cm^{-3}. A cross section of 8 Mb results in a absorption coefficient for the photoionizing radiation of 4 cm^{-1} and a photon mean free path of $\ell_\nu = .25$ cm. Consequently, the radiation is strongly absorbed in air at temperatures near 12,000 ^oK.

This strong absorption indicates the radiation transport in the region $x < 0$ might be adequately represented by the diffusion approximation $\lambda_r \vec{\nabla} T$. Jackson and Nielsen[12] found, however, that this approach yielded values of the energy deposition by re-absorption which were a factor of forty smaller than their numerical calculations. The large discrepancy is due to the rapid temperature variation, near the spark front, over distances on the order of ℓ_ν. As a result the radiation field is highly anisotropic and the diffusion approximation is invalid.

The effect of the absorption at temperatures near 12,000 ^oK is, initially, an increase in the concentrations

of N^+, O^+ and electrons above their equilibrium values. If the relaxation time is short enough, the concentrations will equilibrate to values characteristic of some higher temperature. The net effect of the radiation is then an equilibrium heating of the cold gas, as assumed by Jackson and Nielsen.[12] One reaction which is essential for equilibration is the electron-recombination reaction

$$N^+ + e + M \longrightarrow N + M \qquad \text{(A2.1)}$$

where M is an atomic or molecular species. At electron temperatures near 12,000 ^oK, the reaction rate constants for such reactions are on the order of 10^{-29} cm^6/sec.[27]

There is, however, the competing reaction

$$N^+ + N + M \longrightarrow N_2^+ + M \qquad \text{(A2.2)}$$

for the excess N^+. The constant for this reaction has not been accurately determined. An estimate for temperatures near 12,000 ^oK is $10^{-30 \pm 4}$ cm^6/sec.[27] For equilibrium, atmospheric-pressure air at 12,000 ^oK the nitrogen atom number density is approximately six times the electron number density,[14] so that reaction (A2.2) may proceed at a much faster rate than reaction (A2.1). Consequently, a nonequilibrium concentration of N_2^+ may exist outside the hot plasma core. In fact, investigators[8,20] have reported strong N_2^+ radiation outside the core region. The role of reaction (A2.1) in the relaxation scheme increases with increasing electron number density. The relative

importance of reactions (A2.1) and (A2.2) may change, therefore, as the departure from equilibrium increases.

At 6,000 ^{o}K equilibrium air consists mostly of N_2, N and O, in approximately equal concentrations.[14] Therefore, if the distance in which the temperature drops from 12,000 ^{o}K to 6,000 ^{o}K is on the order of ℓ_ν = .25 cm or less, some radiation can penetrate into the cooler regions and directly photoionize N_2 by the reaction

$$N_2 + h\nu \longrightarrow N_2^+ + e, \quad h\nu \geq 15.6 \text{ ev} \qquad \text{(A2.3)}$$

It is interesting to note that the molecular ions produced by reaction (A2.3) for $h\nu > 18.7$ ev are almost equally distributed among the ground state and the first two excited states, $A\ ^2\prod_u$ and $B\ ^2\sum_u^+$.[24] It is the transition from $B\ ^2\sum_u^+$ to the ground state $X\ ^1\sum_g^+$ which produces the 1st negative band of N_2^+ observed experimentally in References 8 and 20.

A careful study of the reactions which occur subsequent to photoionization is necessary for determining the conditions at the spark front. Reactions related to electron loss or gain are especially important since the absorption of laser radiation is directly related to the electron number density. A major electron loss process is the dissociative recombination of N_2^+

$$N_2^+ + e \longrightarrow 2N \qquad \text{(A2.4)}$$

Its rate constant is on the order of 10^{-7} cm^3/sec.[28]
Three-body recombination

$$X^+ + e + M \longrightarrow X + M \qquad (A2.5)$$

where X is N, O or N_2, also plays a significant role. The reaction rate constant for (A2.5) at electron temperatures near 6,000 ^oK is typically 5×10^{-29} cm^6/sec when M is an atomic or molecular species and 5×10^{-26} cm^6/sec when M is an electron.[27] Electron attatchment to oxygen atoms and molecules may also be important since the negative ions can react with other species to form stable compounds.[29,30]

If the recombination reactions are fast enough, the electron number density will relax to its equilibrium value before the electrons can be appreciably heated by the laser radiation. The assumption of rapid relaxation is made implicitly in the analysis of Jackson and Nielsen.[12] If chemical relaxation occurs too slowly, a nonequilibrium layer will form which will enhance the absorption of laser radiation.

The development of the nonequilibrium layer occurs due to the combined absorption of thermal radiation and laser radiation. The absorption of thermal radiation induces appreciable ionization ahead of the spark analagous to the effect of precursor radiation in shock waves.[31] The free electrons are then selectively heated by inverse

bremsstrahlung absorption of laser radiation and electron thermal conduction. The electrons quickly relax to a Maxwell-Boltzmann distribution at a temperature T_e as a result of the high efficiency of electron-electron collisions in transferring energy. Since the transfer of energy to the heavy particles by electron collisions is inefficient, a two-temperature plasma, with electron temperature exceeding the heavy-particle temperature, develops. Further ionization is then caused by collisions of heavy particles with high-energy electrons. Consequently, an appreciable electron density can exist in a layer ahead of the spark where the temperature of the heavy particles is still quite low.

The inverse bremsstrahlung absorption coefficient, given by Equation (2.4) in Chapter II, is proportional to the square of the electron number density. Therefore, the development of a nonequilibrium layer with a high electron number density ahead of the spark means that absorption of the laser radiation and consequent heating occurs in regions where the heavy-particle temperatures are less than 12,000 ^{o}K.

Although this is a nonequilibrium process, the equilibrium solution obtained in Chapter III can be used to illustrate the effects of the anomalous absorption on spark propagation. Absorption of laser radiation in regions with temperatures less than the equilibrium ignition

temperature can be simulated by lowering the ignition thermal potential to $\theta_i = \theta_i' < .15$ kW/cm. The required laser intensity for a given propagation velocity is then reduced, according to Equation (3.11), to

$$S_o' = \frac{\theta_i'}{.15} S_o$$

where S_o is the intensity calculated using $\theta_i = .15$ kW/cm. Equations (3.6) - (3.10) indicate that the spark thermal potentials are reduced by the same ratio. Therefore, an absorption wave preceding the temperature rise lowers the required laser intensity and the maximum spark temperature for a given propagation velocity.

For example, initiating the absorption at temperatures near 6,000 ^{o}K ($\theta \simeq .025$ kW/cm) results in laser intensities and thermal potentials reduced by a factor of six. Therefore, a free spark of radius .50 cm propagating at 1 m/sec would require only 123 kW/cm^2 and would result in a value of $\bar{T}_m$ = 17,000 ^{o}K. For an ignition temperature of 12,000 ^{o}K, S_o would be 740 kW/cm^2 and $\bar{T}_m$ would exceed 40,000 ^{o}K.

Figure A-1 shows the isotherms for a spark of radius .50 cm propagating at 1 m/sec, assuming $\theta_i = .025$ kW/cm. The effects of convection can be seen in the blunt spark front and elongated isotherms. It is interesting to note that the 12,000 ^{o}K isotherm crosses the x-axis at x = .10 cm.

Since the 6,000 ^{o}K isotherm crosses near x = 0, the width of the zone in which the temperature falls from 12,000 ^{o}K to 6,000 ^{o}K is .10 cm. This distance is less than the absorption length of .25 cm for the vuv radiation emitted from the core. Therefore, the model, though simple, is at least consistent in that the radiation can penetrate to regions where $T < 6{,}000\ ^{o}K$.

The intention of the discussion presented above was to describe, in a qualitative way, the effect re-absorption of thermal radiation would have on spark propagation. A future investigation keying on the processes occurring in the spark front would be useful in understanding the propagation mechanism. In particular, a one-dimensional model of a nonequilibrium gas under the simultaneous influence of two radiation fields would be a logical extension to this analysis.

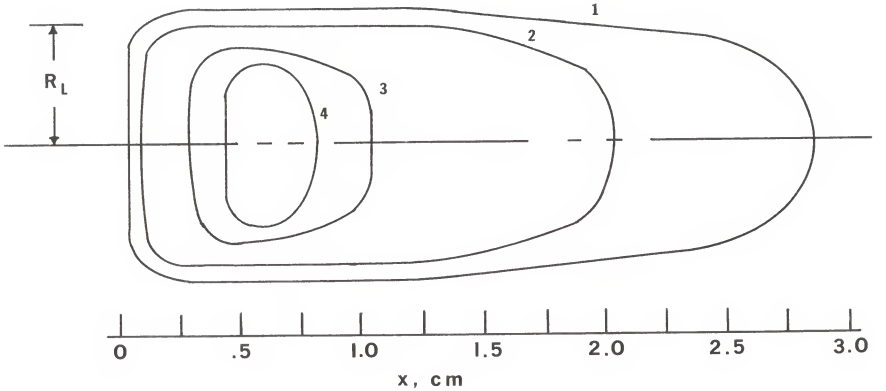

Figure A-1. Isotherms for a Spark with R_L = .50 cm, R_c = 2 R_L, u = 1 m/sec and T_i = 6,000 ^oK. (1) T = 8,000 ^oK, (2) T = 12,000 ^oK, (3) T = 16,000 ^oK, (4) T = 17,000 ^oK.

REFERENCES

1. Buonadonna, V. R., Knight, C. J. and Hertzberg A., "The Laser Heated Hypersonic Wind Tunnel," Aerospace Research Laboratories Report, ARL 73-0074, 1973.

2. Raizer, Y. P., "Breakdown and Heating of Gases under the Influence of a Laser Beam," Sov. Phys.-Usp., 8, 650 (1966).

3. George, E. V., Bekefi, G. and Yaakobi, B., "Structure of a Plasma Fireball Produced by a CO2 Laser," Phys. Fluids, 14, 2708 (1971).

4. Ready, J. F., Effects of High Power Laser Radiation, New York: Academic Press, 1971.

5. Bunkin, F. V., Konov, V. I., Prokhorov, A. M. and Fedorov, V. B., "Laser Spark in the 'Slow Combustion' Regime," JETP-Lett., 9, 371 (1969).

6. Generalov, N. A., Zimakov, V. P., Kozlov, G. I., Masyukov, V. A. and Raizer, Y. P., "Continuous Optical Discharge," JETP-Lett., 11, 302 (1970).

7. Generalov, N. A., Zimakov, V. P., Kozlov, G. I., Masyukov, V. A. and Raizer, Y. P., "Experimental Investigation of a Continuous Optical Discharge," Sov. Phys.-JETP, 34, 763 (1972).

8. Smith, D. C. and Fowler, M. C., "Ignition and Maintenance of a CW Plasma in Atmospheric-pressure Air with CO2 Laser Radiation," Appl. Phys. Lett., 22, 500 (1973).

9. Franzen, D. L., "Continuous Laser Sustained Plasmas," J. Appl. Phys., 44, 1727 (1973).

10. Raizer, Y. P., "Subsonic Propagation of a Light Spark and Threshold Conditions for the Maintenance of Plasma by Radiation," Sov. Phys.-JETP, 31, 1148 (1970).

11. Hall, R. B., Maher, W. E. and Wei, P. S. P., "An Investigation of Laser-Supported Detonation Waves," Air Force Weapons Laboratory Technical Report AFWL-TR-73-28, 1973.

12. Jackson, J. P. and Nielsen, P. E., "Role of Radiative Transport in the Propagation of Laser Supported Combustion Waves," AIAA Paper No. 74-228, 1974.

13. Zeldovich, Y. B. and Raizer, Y. P., Physics of Shock Waves and High Temperature Hydrodynamic Phenomena Vol. 1, edited by W. D. Hayes and R. F. Probstein, New York: Academic Press, 1966.

14. Wei, P. S. P. and Hall, R. B., "Emission Spectra of Laser Supported Detonation Waves," J. Appl. Phys., 44, 2311 (1973).

15. Luke, Y. L., "Integrals of Bessel Functions," Handbook of Mathematical Functions, edited by M. Abramowitz and I. A. Stegun, Washington, D.C.: U.S. Government Printing Office, 1966.

16. Hermann, W. and Schade, E., "Transportfunktionen von Stickstoff bis 26000 °K," Z. Physik, 233, 333 (1970).

17. Hermann, W. and Schade, E., "Radiative Energy Balance in Cylindrical Nitrogen Arcs," J. Quant. Spectrosc. Radiat. Transfer, 12 1257 (1972).

18. Raizer, Y. P., "Propagation of Discharges and Maintenance of a Dense Plasma by Electromagnetic Fields," Sov. Phys.-Usp., 15, 688 (1973).

19. Fowler, M. C., Smith, D. C., Brown, C. O. and Radley, R. J., "Laser Supported Absorption Waves," United Aircraft Research Laboratories Report No. N921716-9, 1974.

20. Keefer, D. R., Henriksen, B. B. and Braerman, W. F., "Experimental Study of a Stationary Laser Produced Air Plasma," to be published.

21. Olver, F. W. J., "Bessel Functions of Integer Order," Handbook of Mathematical Functions, edited by M. Abramowitz and I. A. Stegun, Washington, D.C.: U.S. Government Printing Office, 1966.

22. Widder, D. V., Advanced Calculus (2nd Edition), Englewood Cliffs, N.J.: Prentice Hall, Inc., 1961.

23. Penner, S. S. and Olfe, D. B., Radiation and Reentry, New York: Academic Press, 1968.

24. Huffman, R. E., "Photochemical Processes: Cross-Section Data," Reaction Rate Handbook (2nd Edition), edited by M. H. Bortner and T. Baurer, Santa Barbara, Calif.: DASIAC, DoD Nuclear Information and Analysis Center, 1972.

25. Wilson, K. H. and Nicolet, W. E., "Spectral Absorption Coefficients of Carbon, Nitrogen and Oxygen Atoms," J. Quant. Spectrosc. Radiat. Transfer, 12, 1257 (1972).

26. Samson, J. A. R. and Cairns, R. B., "Absorption and Photoionization Cross Sections of O2 and N2 at Intense Solar Lines," J. Geophys. Res., 69, 4583 (1964).

27. Bortner, M. H., Kummler R. H. and Baurer, T., "Summary of Suggested Rate Constants," Reaction Rate Handbook (2nd Edition), edited by M. H. Bortner and T. Baurer, Santa Barbara, Calif.: DASIAC, DoD Nuclear Information and Analysis Center, 1972.

28. Bardsley, J. N. and Biondi, M. A., "Dissociative Recombination," Advances in Atomic and Molecular Physics Volume 6, edited by D. R. Bates and I. Esterman, New York: Academic Press, 1970.

29. Phelps, A. V., "Electron Attachment and Detachment Processes," Reaction Rate Handbook (2nd Edition), edited by M. H. Bortner and T. Baurer, Santa Barbara, Calif.: DASIAC, DoD Nuclear Information and Analysis Center, 1972.

30. Ferguson, E., "Ion-Neutral Reactions A. Thermal Processes," Reaction Rate Handbook (2nd Edition), edited by M. H. Bortner and T. Baurer, Santa Barbara, Calif.: DASIAC, DoD Nuclear Information and Analysis Center, 1972.

31. Ferrari, C. and Clarke, J. H., "On Photoionization Ahead of a Strong Shock Wave," Supersonic Flow, Chemical Processes and Radiative Transfer, edited by D. B. Olfe and V. Zakkay, New York: Pergamon Press, 1964.

BIOGRAPHICAL SKETCH

Jad Hanna Batteh was born in Ramallah, Jordan, on January 5, 1947. After graduating from Ribault Senior High School of Jacksonville, Florida, in June, 1964, he enrolled at the University of Florida. As an undergraduate, he was elected to membership in Phi Eta Sigma, Sigma Tau and Tau Beta Pi honorary fraternities. He received the degree of Bachelor of Science in Aerospace Engineering with High Honors in December, 1967.

Beginning July, 1968, he was employed for two and a half years as an aircraft structures engineer at the Lockheed-Georgia Company in Marietta, Georgia. During that time, he attended the Georgia Institute of Technology from which he received the degree of Master of Science in Aerospace Engineering in December, 1970.

Since the fall of 1971, he has been enrolled in the Graduate School of the University of Florida. During his tenure, he has held an NDEA Fellowship and a Graduate School Fellowship.

He is married to the former Jane Joseph Bateh of Jacksonville, Florida.

I certify that I have read this study and that in my opinion it conforms to acceptable standards of scholarly presentation and is fully adequate, in scope and quality, as a dissertation for the degree of Doctor of Philosophy.

Dennis R. Keefer, Chairman
Associate Professor of
Engineering Sciences

I certify that I have read this study and that in my opinion it conforms to acceptable standards of scholarly presentation and is fully adequate, in scope and quality, as a dissertation for the degree of Doctor of Philosophy.

Bernard M. Leadon
Professor of Engineering
Sciences

I certify that I have read this study and that in my opinion it conforms to acceptable standards of scholarly presentation and is fully adequate, in scope and quality, as a dissertation for the degree of Doctor of Philosophy.

Ulrich H. Kurzweg
Associate Professor of
Engineering Sciences

I certify that I have read this study and that in my opinion it conforms to acceptable standards of scholarly presentation and is fully adequate, in scope and quality, as a dissertation for the degree of Doctor of Philosophy.

Robert G. Blake
Associate Professor of
Mathematics

I certify that I have read this study and that in my opinion it conforms to acceptable standards of scholarly presentation and is fully adequate, in scope and quality, as a dissertation for the degree of Doctor of Philosophy.

John W. Flowers
Professor of Physics
and Astronomy

This dissertation was submitted to the Dean of the College of Engineering and to the Graduate Council, and was accepted as a partial fulfillment of the requirements for the degree of Doctor of Philosophy.

August, 1974

Dean, College of Engineering

Dean, Graduate School

1853